2006-08-21

Unscented Kalman Filtering: NPSAT1 Ground Test Results

Gong, Qi; Ross, Michael I.

The American Institute of Aeronautics and Astronautics (AIAA)

https://hdl.handle.net/10945/29685

AIAA Guidance, Navigation, and Control Conference and Exhibit
21 - 24 August 2006, Keystone, Colorado

AIAA 2006-6352

Unscented Kalman Filtering: NPSAT1 Ground Test Results

Pooya Sekhavat, [¤] Qi Gong [y] and I. Michael Ross [z]

NPSAT1 is a small satellite that employs magnetic sensing and actuation for attitude control. The spacecraft orientation and angular velocity should, therefore, be estimated from the magnetometer readings. The inherent nonlinear dynamics of the system poses a challenging problem on the observer design. This paper demonstrates the ground test results of NPSAT1 state estimation using the Unscented Kalman Filter (UKF) - a fairly recent method with inherent appeals of extended Kalman filter but with no need for linearization; thus more suitable for highly nonlinear filtering and control applications. The quaternion-based modeling constraint that the quaternion has a unit norm is enforced by treating the norm of the quaternion as a dummy measurement. The experimental results show the superior performance of the UKF in practice.

I. Introduction

NPSAT1 is a small experimental satellite designed and constructed at the Naval Postgraduate School and is scheduled to launch in 2007 (Fig. 1). The satellite is a prolate non-spinning body that primarily uses a three-axis active magnetic attitude control. Magnetic attitude control facilitates the system robustness, light weight, low power consumption, and cost-efficiency and is an attractive choice for low-orbit satellites. The NPSAT1 magnetic control system is comprised of a magnetometer and three magnetic torque rods. Interaction between the three magnetic dipole moments generated by the torque rods and the Earths magnetic field produces a resulting torque that actuates the spacecraft. As far as the previous literature on magnetic attitude control[1–5] and, in particular, magnetic attitude control for NPSAT1[6,7] is concerned, the control command is generated using the current spacecraft position and/or angular velocity. Having a magnetometer as the only available sensor onboard, rules out any possibility of direct position and/or velocity measurement. Therefore, it is imperative to estimate them using magnetometer readings.

One of the most powerful estimation techniques that has been commonly used in various dynamic systems is the Kalman filter, initially designed for linear systems and later extended for nonlinear systems (EKF). The EKF design is based on linearizing the system dynamics along the system trajectory and applying standard linear Kalman Filter to get the estimation. This enables a better capture of the nonlinear characteristics of the system during the state estimation and, thus, be potentially attractive for spacecraft attitude control with dominant nonlinear characteristics.[8–11]

While EKF serves as a popular tool for nonlinear estimation, it continues to endure some of the fundamental limitations of the original Kalman filter. In particular, the linearization inherent in the EKF algorithm can be the potential cause of ultimate divergence and failure of the scheme. Moreover, derivation of Jacobian matrix for complex nonlinear systems can be cumbersome and prone to human errors.

As a major step forward, Julier and Uhlmann proposed the so-called Unscented Kalman filter (UKF),[12,13] that circumvents the above-mentioned problems. The UKF is "founded on the intuition that it is easier to approximate a probability distribution than it is to approximate an arbitrary nonlinear function or transformation".[12] By introducing a set of sample points, called sigma-points, that capture the higher order statistics of the system, UKF successfully avoids the EKF's linearization step. This property alone provides significant advantage by extending the application of the method to systems with discontinuity, table look

[*]Postdoctoral Associate, Department of Mech. & Astro., Naval Postgraduate School, Monterey, CA 93943, E-mail: psekhava@nps.edu.

[†]Postdoctoral Associate, Department of Mech. & Astro., Naval Postgraduate School, Monterey, CA 93943, E-mail: qgong@nps.edu.

[‡]Professor, Department of Mechanical and Astronautical Engineering, Naval Postgraduate School, Monterey, CA, 93943, Email: imross@nps.edu

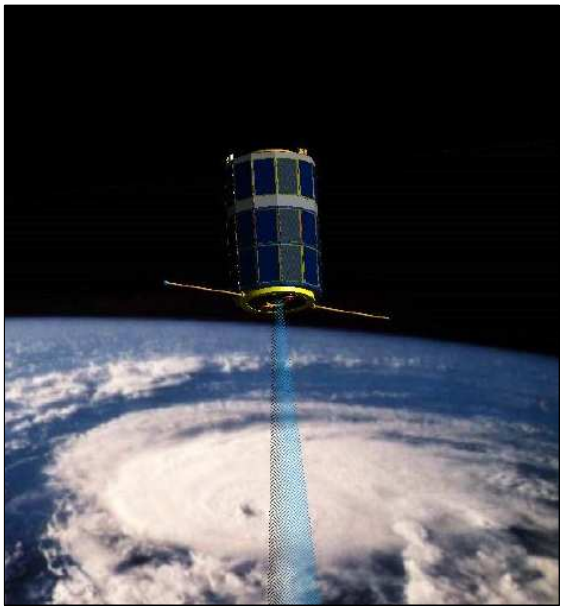

Figure 1. Rendition of NPSAT1 in orbit.

up, or even systems with rule-based decision making where Extended Kalman Filter is not applicable. Furthermore, by preserving the higher order information of the system, UKF improves both the accuracy as well as the convergence properties of the estimated results. Remarkably, it has been shown that UKF has roughly the same computational complexity as the EKF[14,15] and its superior performance can be achieved with no extra computational burden.

Within the context of attitude estimation, UKF has been recently applied for attitude estimation of spacecraft without considering the effects of magnetic actuation.[15–17] The numerical simulations presented in these studies have illustrated the superior performance of UKF in spacecraft attitude estimation. In the present work, we extend the application of UKF to magnetically actuated spacecraft and, both theoretically and experimentally, demonstrate its successful performance for attitude estimation.

Typically, the attitude state is represented by a quaternion vector to prevent singularity at certain attitudes. Since the norm of the quaternion vector is always equal to one, this method of state representation introduces an additional constraint on the attitude states that should be enforced during any state estimation. In case of using EKF or UKF for attitude estimation, failure to do so may cause the covariance matrix of the quaternion state to be singular.[8] The common remedy used in previous studies is to replace the four element quaternion with a newly defined three-element error quaternion.[8–10,15,16,18] In this paper, we adopt a new simple strategy to impose the unity-norm constraint of the quaternion. Simply put, we treat the norm of the quaternion as a dummy output. In other words, although there is no real sensor to measure the norm of the quaternion vector, we know its "sensed" value is always equal to one from physics. Therefore, we can augment the norm of the quaternion to the real sensor measurements and proceed with the standard UKF algorithm. In this paper we show that this simple idea resolves the unity-norm constraint issues in very easy way that is desirable for real-time experimental implementations.

The paper is organized as follows. First, we illustrate the performance of the proposed method of incorporating the unity-norm of quaternion vector through NPSAT1 simulations. We then take the next step of examining UKF algorithm in practice through NPSAT1 ground tests. To verify the convergence of estimation routine, the estimated attitude states are compared with an alternative set of independently measured values obtained from an optical measurement system installed on the test rig. The experimental ground test results not only confirm the previous numerical works on UKF advantages in attitude estimation,[15–17] but also illustrate its successful performance in the particular case of highly nonlinear magnetic actuation systems.

II. Dynamic Model of NPSAT1

In this section we briefly describe the dynamics of the NPSAT1 spacecraft. The details can be found in Ref. [7,19]. Choosing the standard quaternion and body rates as the state variables, we have $x = (q, \omega) \in \mathbb{R}^7$, where

- $q = (q_1, q_2, q_3, q_4)$: quaternion of the body frame with respect to the orbit frame,
- $\omega = (\omega_x, \omega_y, \omega_z)$: rotation rate of the body frame with respect to the inertial frame expressed in the body frame.

and the quaternion must lie on S^3 given by the following state constraint at each time instant

$$q_1^2 + q_2^2 + q_3^2 + q_4^2 = 1 \tag{1}$$

Following the above notations, the kinematic equations of motion for the NPSAT1 is[19]

$$\begin{aligned}
\dot{q}_1(t) &= \frac{1}{2}\left[\omega_x(t)q_4(t) - \omega_y(t)q_3(t) + \omega_z(t)q_2(t) \right. \\
&\quad \left. +\omega_0 q_3(t)\right] && (2)\\
\dot{q}_2(t) &= \frac{1}{2}\left[\omega_x(t)q_3(t) + \omega_y(t)q_4(t) - \omega_z(t)q_1(t) \right. \\
&\quad \left. +\omega_0 q_4(t)\right] && (3)\\
\dot{q}_3(t) &= \frac{1}{2}\left[-\omega_x(t)q_2(t) + \omega_y(t)q_1(t) + \omega_z(t)q_4(t) \right. \\
&\quad \left. -\omega_0 q_1(t)\right] && (4)\\
\dot{q}_4(t) &= \frac{1}{2}\left[-\omega_x(t)q_1(t) - \omega_y(t)q_2(t) - \omega_z(t)q_3(t) \right. \\
&\quad \left. -\omega_0 q_2(t)\right] && (5)
\end{aligned}$$

where ω_0 is angular velocity of the orbit with respect to the inertial frame.

Euler's equations can next be used to derive the dynamic equations of motion. Control torques are applied as a result of the interaction between the dipole moments generated by the three magnetic torque rods $u = (u_1, u_2, u_3) \in \mathbb{R}^3$ and the Earth magnetic field. Thus,

$$\begin{aligned}
\dot{\omega}_x(t) &= \frac{I_2 - I_3}{I_1}[\omega_y(t)\omega_z(t) - 3\frac{\mu}{r_0^3}C_{23}C_{33}] + \\
&\quad \frac{1}{I_1}\left[B_z(q,t)u_2 - B_y(q,t)u_3\right] && (6)\\
\dot{\omega}_y(t) &= \frac{I_3 - I_1}{I_2}[\omega_x(t)\omega_z(t) - 3\frac{\mu}{r_0^3}C_{13}C_{33}] + \\
&\quad \frac{1}{I_2}\left[B_x(q,t)u_3 - B_z(q,t)u_1\right] && (7)\\
\dot{\omega}_z(t) &= \frac{I_1 - I_2}{I_3}[\omega_x(t)\omega_y(t) - 3\frac{\mu}{r_0^3}C_{13}C_{23}] + \\
&\quad \frac{1}{I_3}\left[B_y(q,t)u_1 - B_x(q,t)u_2\right] && (8)
\end{aligned}$$

where (I_1, I_2, I_3) are the principal moments of inertia; μ is Earth gravitational constant; r_0 is the distance from the center of spacecraft to the center of the Earth and C_{ij} denote the corresponding element in the Direction Cosine Matrix

$$C_q = \begin{bmatrix} q_1^2 - q_2^2 - q_3^2 + q_4^2, & 2(q_1q_2 + q_3q_4), & 2(q_1q_3 - q_2q_4) \\ 2(q_1q_2 - q_3q_4), & q_2^2 - q_1^2 - q_3^2 + q_4^2, & 2(q_2q_3 + q_1q_4) \\ 2(q_1q_3 + q_2q_4), & 2(q_2q_3 - q_1q_4), & q_3^2 - q_1^2 - q_2^2 + q_4^2 \end{bmatrix}.$$

Also, (B_x, B_y, B_z) are Earth's magnetic field in the body frame defined as

$$\begin{pmatrix} B_x(q,t) \\ B_y(q,t) \\ B_z(q,t) \end{pmatrix} = C_q \begin{pmatrix} B_1(t) \\ B_2(t) \\ B_3(t) \end{pmatrix} \tag{9}$$

where $(B_1(t), B_2(t), B_3(t)$ are the components of the Earth's magnetic field in the orbit frame and can be modeled as[20]

$$\begin{aligned} B_1 &= \frac{M_e}{r_0^3}[\cos(\omega_0 t)[\cos(\epsilon)\sin(i) - \sin(\epsilon)\cos(i)\cos(\omega_e t)] \\ &\quad - \sin(\omega_0 t)\sin(\epsilon)\sin(\omega_e t)] \\ B_2 &= -\frac{M_e}{r_0^3}[\cos(\epsilon)\cos(i) + \sin(\epsilon)\sin(i)\cos(\omega_e t)] \\ B_3 &= \frac{2M_e}{r_0^3}[\sin(\omega_0 t)[\cos(\epsilon)\sin(i) - \sin(\epsilon)\cos(i)\cos(\omega_e t)] \\ &\quad + 2\cos(\omega_0 t)\sin(\epsilon)\sin(\omega_e t)]. \end{aligned}$$

For NPSAT1, the parameters used in the above equations are as follows:

- $(I_1, I_2, I_3) \approx (5, 5.1, 2) kg.m^2$
- $\omega_0 = \sqrt{\frac{\mu}{r_0^3}} \approx 0.00108 rad/s$
- $\mu = 3.98601 \times 10^{14} m^3/s^2$
- $r_0 = 6978 \pm 40 km$
- $M_e = 7.943 \times 10^{15} Wb.m$; the magnetic dipole moment of the Earth
- $i = 35.4^\circ$; the orbit inclination
- $\epsilon = 11.7^\circ$; is the magnetic dipole tilt
- $\omega_e = 7.29 \times 10^{-5} rad/s$; is the spin rate of the Earth.

The complete dynamic model of NPSAT1 is given by equations (2)—(8). Clearly, it is a fairly complex nonlinear system. Note that the magnetic field, $(B_1(t), B_2(t), B_3(t))$, is time-variant. Therefore, the overall system is a time-varying dynamic system. Also, the maximum applicable control torque is subject to the limitations on the available dipole moments, i.e.,

$$|u_i| \leq 33 A.m^2, \qquad i = 1, 2, 3.$$

NPSAT1 does not have any sensor for direct measurement of the state variables, (q, ω). In fact, the only onboard sensor is a three-axis magnetometer that measures the magnetic field in the body frame. However, since the NPSAT1 attitude control is through active actuation of magnetic torque rods, the magnetometer reading at each time instant is a combination of the Earth magnetic field, (B_x, B_y, B_z), and the magnetic field generated by actuators, (B_{xu}, B_{yu}, B_{zu}). Thus, the output function of the system (2)—(8) is

$$h(q, \omega, u, t) = \begin{pmatrix} B_x(q,t) \\ B_y(q,t) \\ B_z(q,t) \end{pmatrix} + \begin{pmatrix} B_{xu}(u_1, u_2, u_3) \\ B_{yu}(u_1, u_2, u_3) \\ B_{zu}(u_1, u_2, u_3) \end{pmatrix} \tag{10}$$

On the other hand, the magnetic filed generated by each actuator, (B_{xu}, B_{yu}, B_{zu}), is a linear function of the actuator dipole moment, (u_1, u_2, u_3),[21]

$$B_{u_k} = \frac{\mu_0 u_k}{2\pi Z^3} \qquad k = 1, 2, 3.$$

where Z is the distance normal to the coil, and μ_0 is the permeability constant. Therefore, knowing the control moment, u_k, and the slope of the linear functions $B_{u_k} = f(u_k)$, we can then calculate and subtract B_{u_k} from the sensor measurements to obtain the pure Earth magnetic field, (B_x, B_y, B_z).

III. Unscented Kalman Filter Design for NPSAT1

As explained in previous sections, the major difference between an EKF and a UKF lies in the prediction step of the filter. EKF uses linearization technique to propagate the mean and the covariance while UKF utilizes the so-called sigma point in order to generate the prediction. This elimination of linearization step helps UKF provide improved accuracy over the EKF. This is due to the fact that the linearization step of the EKF scheme only preservers the first order system statistics. On the other hand, the UKF sigma point propagation preserves both the first- and second-order statistics and results in considerably improved convergence properties. This is particularly important for highly nonlinear systems like NPSAT1 where poor convergence of the estimator can degrade the stability of the closed-loop control system and eventually make the system unstable. Therefore, in this study, UKF is adopted for observer design. The details of the standard UKF algorithm is included in the Appendix. More details can be found in the Refs. [12, 13, 15].

While UKF has served as an accurate and efficient tool for nonlinear observer design, we cannot enforce the constraint equation (1) by employing the standard UKF algorithm for attitude estimation. As a result of not enforcing such constraint equation, the covariance matrix of the quaternion state will be singular.[8] Since this has also been a problem in EKF applications for attitude estimation, it has been previously addressed and various solutions has been proposed in the literature. For example, in Ref.[15] the problem is addressed via employing a three-element error-quaternion state for attitude representation. In the present work, we adopt a simple new strategy that requires less computations and, thus, is more suitable for real-time implementations.

Consider a general nonlinear system

$$\dot{x} = f(x, u, t) \tag{11}$$

with measurement output

$$y = h(x, u, t)$$

and algebraic constraint

$$\phi(x, u, t) = 0$$

that should always be satisfied along the system trajectory. In other words, although there is no real sensor to measure the quantity $\phi(x, u, t)$, we know that it must be zero at all times. This means that $\phi(x, u, t)$ can be treated as a dummy output and be augmented into the real measurements. We can, then, construct a new output function

$$\tilde{y} = \begin{pmatrix} h(x, u, t) \\ \phi(x, u, t) \end{pmatrix} \tag{12}$$

and proceed with the standard UKF and EKF observer design technique. This strategy provides a simple way to incorporate the constraint information into the filter design procedure with no need for state transformation. Note that, when the filter converges, the algebraic constraint (1) is automatically enforced. This method of enforcing the unity-norm constraint of quaternion is extremely simple to implement and does not require any modification in the standard UKF/EKF routine.

By applying the above-explained idea for the state estimation of NPSAT1, we construct the following augmented output function

$$h(q, \omega, u, t) = \begin{pmatrix} B_x(q, t) + B_{xu}(u_1, u_2, u_3) \\ B_y(q, t) + B_{yu}(u_1, u_2, u_3) \\ B_z(q, t) + B_{zu}(u_1, u_2, u_3) \\ q_1^2 + q_2^2 + q_3^2 + q_4^2 - 1 \end{pmatrix} \tag{13}$$

Equations (13) can now be replaced into the left-hand side of (9) and then used in conjunction with dynamic equations (2)—(8) in the standard UKF algorithm (see Appendix).

IV. Simulation Results

Before proceeding with experiments, the above explained method is simulated with the actual NPSAT1 parameters detailed in section II. The simulation results with zero control input are shown in Fig.2 and Fig.3. In these simulations, the actual initial orientation of the spacecraft in all three directions is 45° and the actual initial angular velocities are $(\omega_x, \omega_y, \omega_z) = (0.002, 0.03, 0.02)\ rad/s$. However, the filter starts with the initial orientation of 90° in all three directions and the initial angular velocities of $(\omega_x, \omega_y, \omega_z) = (0.004, 0.06, 0.04)$ rad/s. In other words, the initial state errors are deliberately chosen to be 100% larger than their actual real values. It is clearly seen that despite such a large initial errors, all states converge to their real values.

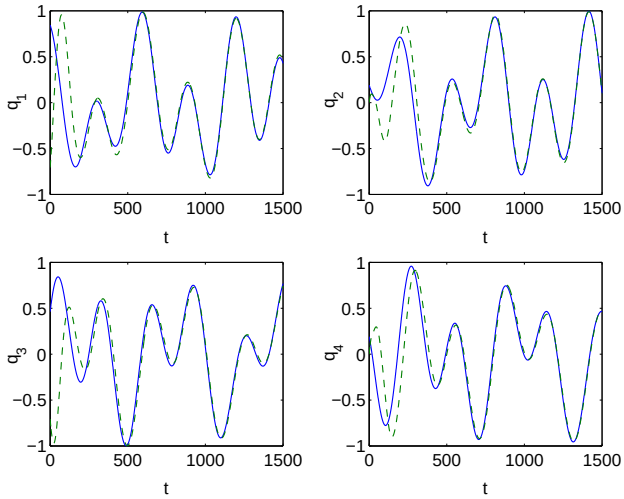

Figure 2. Quaternion estimation for NPSAT1. The solid lines are the real and the dashed lines are the estimated values.

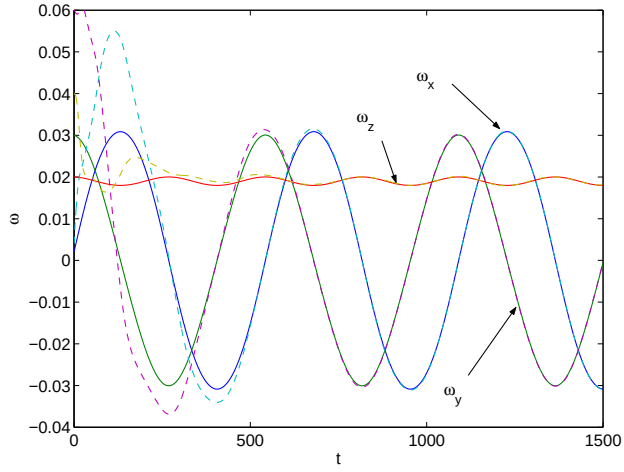

Figure 3. Angular velocity estimation for NPSAT1. The solid lines are the real and the dashed lines are the estimated values.

In order to better follow the trend of state convergence, Fig.3 illustrates the state estimation error defined as

$$\begin{aligned}\|e(t)\|^2 &= \|q_1 - \hat{q}_1\|^2 + \|q_2 - \hat{q}_2\|^2 + \|q_3 - \hat{q}_3\|^2 + \\ &\quad \|q_4 - \hat{q}_4\|^2 + \|\omega_x - \hat{\omega}_x\|^2 + \|\omega_y - \hat{\omega}_y\|^2 \\ &\quad + \|\omega_z - \hat{\omega}_z\|^2.\end{aligned}$$

It is clear that the error converges to zero despite such an unrealistically large initial estimation errors.

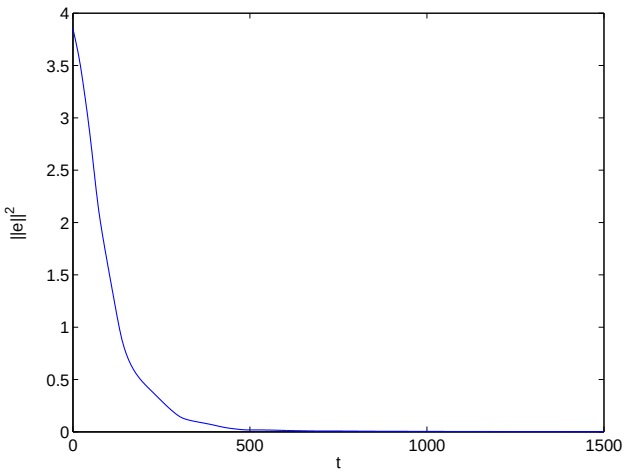

Figure 4. Estimation error.

V. Ground Test Experiments

As it is not easy to create an artificial space-like environment on the surface of the Earth, an air-bearing platform is used to resemble NPSAT1 during the ground tests. The experimental results presented in this section are part of the extensive test experiments conducted before the NPSAT1 launch. They are intended to specifically address the applicability of the proposed UKF procedure in practical maneuvers.

A. Experimental Test Rig

Figure 5 illustrates the air-bearing test rig. The table is capable of moving about three perpendicular axes that resemble the NPSAT1 attitude motion in orbit. The table stand is secured on a floor covered with electrically-safe rubber matting. The platform is equipped with on-board power supply comprised of four 12-volt and two 6-volt batteries. Three MT-30-2-CGS Microcosm magnetic torque rods are aligned with the principle axes of the air-bearing. The test-bed also includes a Honeywell Smart Digital Magnetometer HMR2300 aligned with the principle axes of the air-bearing. The magnetometer measures the instantaneous magnetic field in each x-y-z direction. The onboard single-board computer (SBC) is a repackaged PC running a 400 MHz Pentium. The air-bearing Input/Output (I/O) is orchestrated with a simple onboard microcontroller which accepts ASCII-encoded serial-based (RS232) commands. The SBC interfaces with the magnetometer and the torque control board via serial commands and the microcontroller. The SBC is connected to the command-generating Laptop by serial communication through a Linksys wireless Ethernet bridge. The communication is facilitated by using the Matlab Instrument Control Toolbox. The overall platform is symmetrical and is passively balanced by using dummy weights that are installed symmetric to the actual components such as magnetic torque rods, magnetometer, wireless bridge, etc.

The UKF algorithm only uses the magnetometer readings for state estimation. In order to validate the UKF estimated states, the air-bearing is also equipped with an optical measurement system that independently measures the attitude angles. It consists of an onboard laser diode, and indicator screen, CCD camera and a PC with the required software to transform the camera readings into Euler angles.

B. Modified Air-bearing Dynamic Equations

As a result of using the air-bearing platform for test experiments, the original NPSAT1 equations of motion (2)—(8) should be modified based on the air-bearing dynamic features. The main difference in the actual NPSAT1 and the laboratory test rig is the fact that the dynamic equations of NPSAT1 are derived with respect to the spacecraft center of mass whereas the air-bearing equations are with respect to its center of rotation which normally does not coincide with its center of mass. Consequently, the in-flight gravity

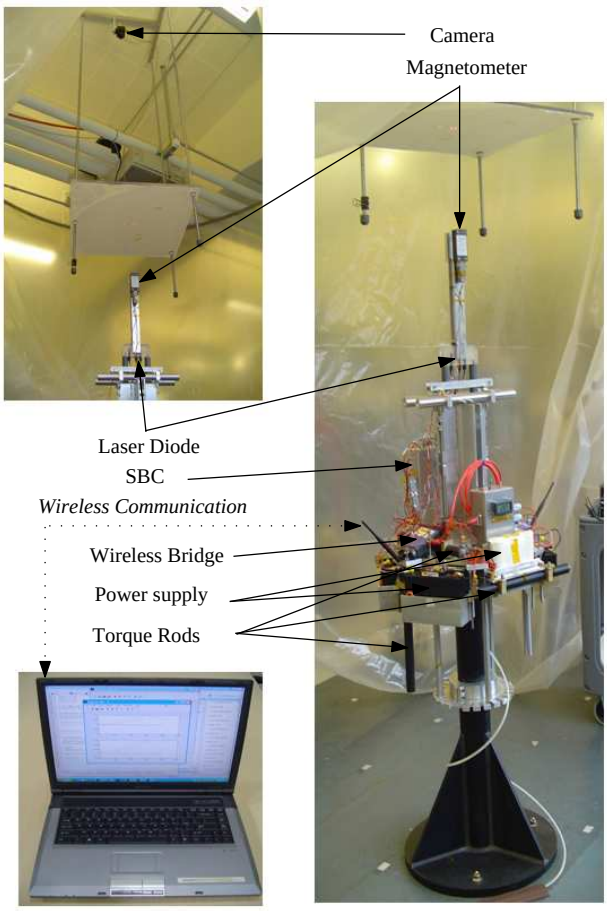

Figure 5. Air-bearing test rig.

gradient torque is replaced with the following external gravitational torque:

$$\begin{bmatrix} T_x \\ T_y \\ T_z \end{bmatrix} = mgl \begin{bmatrix} -C_{23} \\ C_{13} \\ 0 \end{bmatrix},$$

where m is the mass of the table platform, g is the gravitational constant and l is the distance between the center of mass and the center of rotation of the table. This results in the modified dynamic equations (6)—(8) as follows:

$$\dot{\omega}_x(t) = \frac{I_2 - I_3}{I_1}\omega_y(t)\omega_z(t) - \frac{mglC_{23}}{I_1} + \frac{1}{I_1}\left[B_z(q,t)u_2 - B_y(q,t)u_3\right] \quad (14)$$

$$\dot{\omega}_y(t) = \frac{I_3 - I_1}{I_2}\omega_x(t)\omega_z(t) + \frac{mglC_{13}}{I_2} + \frac{1}{I_2}\left[B_x(q,t)u_3 - B_z(q,t)u_1\right] \quad (15)$$

$$\dot{\omega}_z(t) = \frac{I_1 - I_2}{I_3}\omega_x(t)\omega_y(t) + \frac{1}{I_3}\left[B_y(q,t)u_1 - B_x(q,t)u_2\right] \quad (16)$$

Equations (14)—(16) together with (2)—(5) constitute the complete dynamic model for the airbearing test-bed. The airbearing parameters used in the above dynamic equations are listed in Table B.

(I_1, I_2, I_3)	$(2.6, 2.87, 1.45) kg \cdot m^2$
m	$59kg$
l	$0.56mm$

Table 1. Parameters of the air-bearing test-bed

Finally, as explained in section III, the magnetometer measurements are combination of the Earth's magnetic field (B_x, B_y, B_z) and the magnetic field generated when actuators are in action, (B_{xu}, B_{yu}, B_{zu}). In order to derive the real values of the Earth magnetic field, the latter magnetic contamination should be calculated and subtracted from the measurements. A simple experimental analysis reveals that the linear relation between the actuator-generated magnetic field and the actuator control signal can be expressed as follows

$$\begin{aligned} B_{xu}(u_1, u_2, u_3) &= -0.0012u_1 - 0.000039u_2 - 0.00051u_3 \\ B_{yu}(u_1, u_2, u_3) &= -0.000013u_1 - 0.0017u_2 - 0.00011u_3 \\ B_{zu}(u_1, u_2, u_3) &= 0.000049u_1 - 0.00022u_2 + 0.0017u_3 \end{aligned}$$

C. Results and Analysis

In the the first set of experiments, we apply a constant control

$$u_1 = u_2 = u_3 = 33A/m^2$$

to the system and estimate the system states using the explained UKF algorithm. The only measurement available to the UKF is the magnetic field measured from the magnetometer. The motion starts when the spacecraft is oriented near $(q_1, q_2, q_3, q_4) = (0, 0, 0, 1)$. However, similar to the simulations discussed in Sec IV, the filter starts with large initial errors of $(q_1, q_2, q_3, q_4) = (0.4, -0.2, 0.1, 0.9)$. In fact, the filter initial conditions do not even satisfy the unity-norm condition of equation (1). The UKF estimated quaternion and angular velocities are depicted in Figs. 6 and 7, respectively.

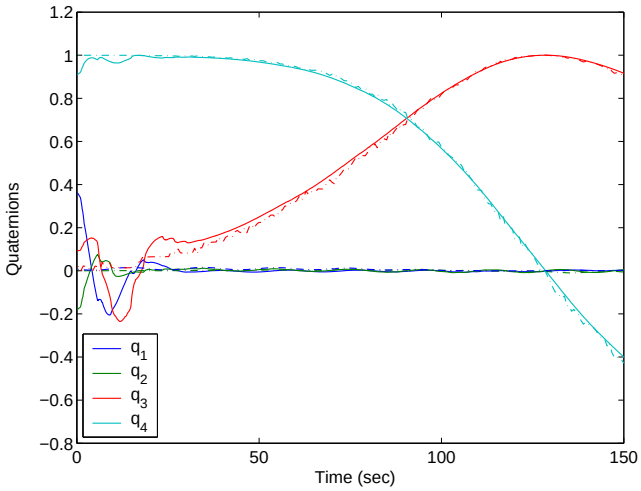

Figure 6. UKF Estimated quaternion. Solid lines represent the estimations and dashed lines are the laser diode measurements.

Next, the convergence of the filter is verified in two different and completely independent ways. The first verification method is to compare the UKF estimated quaternion with the camera angular measurements. Although neither quaternion nor the angular rates can be measured during NPSAT1 mission in orbit, the

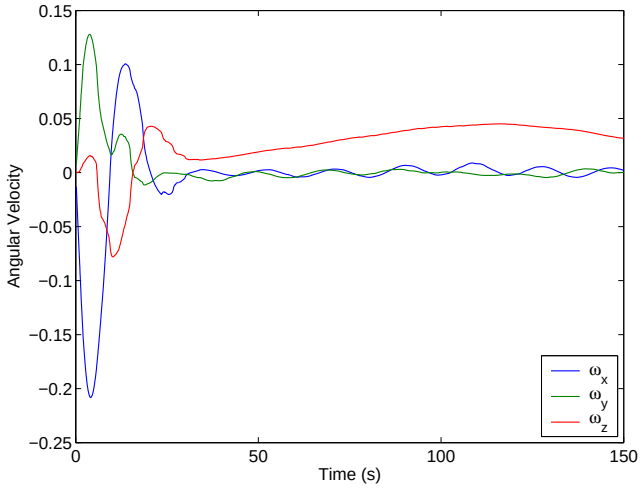

Figure 7. UKF Estimated angular velocities.

ground test-bed is equipped with a CCD camera capable of recording the Euler angles (θ, ϕ, ψ) throughout the motion. The Euler angles can then be transformed to quaternion by employing

$$\begin{bmatrix} q_1 \\ q_2 \\ q_3 \\ q_4 \end{bmatrix} = \begin{bmatrix} \sin(\theta/2)\cos((\phi-\psi)/2) \\ \sin(\theta/2)\sin((\phi-\psi)/2) \\ \cos(\theta/2)\sin((\phi+\psi)/2) \\ \cos(\theta/2)\cos((\phi+\psi)/2) \end{bmatrix}$$

The result of such measurement and transformations are the dotted lines included in Fig. 6. It can be seen that the estimated and camera-measured quaternion coincides within the camera's precision of 2.5°.

As a second measure of convergence, we calculate the right-hand side of equation (9) using the UKF estimated states. If convergence is achieved, the UKF-based calculated right-hand side values for the magnetic field should match the experimental measurements of magnetometer (left-hand side). This is shown in Fig. 8. The excellent match between the two is another indication that the estimation scheme has indeed converged.

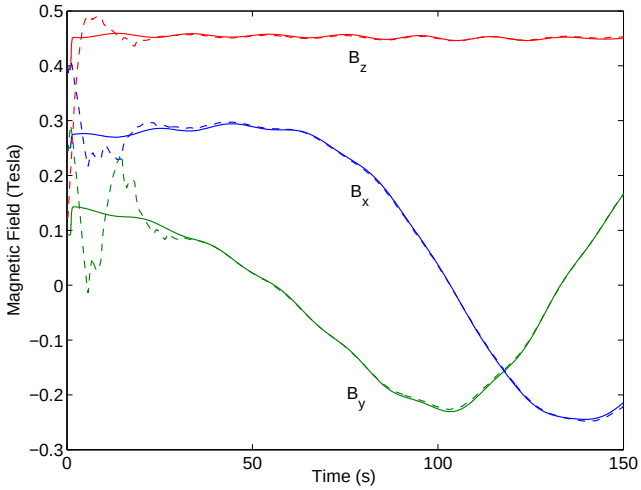

Figure 8. The magnetic field. Solid lines are the measurement from the magnetometer and the dashed lines are the estimated values based on UKF estimated states.

To further illustrate that despite the initial violation of the quaternion norm from unity, the filter convergence will automatically enforce the unity of the quaternion norm, the norm of the estimated quaternion

is depicted in Fig. 9. It verifies that the quaternion is preserved to be one after the filter convergence is achieved.

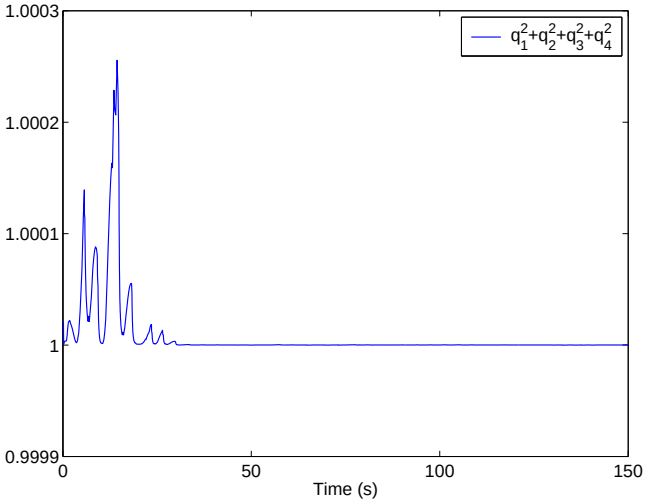

Figure 9. The norm of the estimated quaternion.

In the second set of experiments, we test the practical performance of the UKF scheme under the time-varying control trajectory shown in Fig.10. It is the open-loop control for 135° time-optimal slew maneuver of the spacecraft about its z-axis. The details of how the control trajectory is derived is beyond the scope of this paper and is discussed elsewhere.[19]

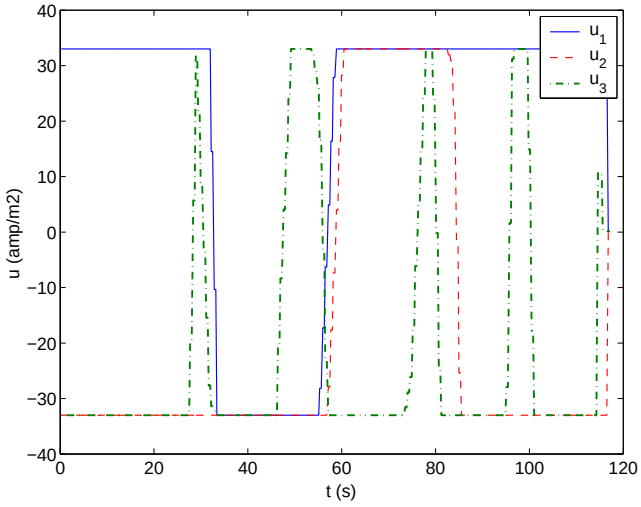

Figure 10. The time-varying control been applied.

Figs. 11 and 12 show the UKF estimated states under the above time-varying control trajectory. Similar to the the previous case with constant control, two independent tests are conducted to verify the successful convergence of the filter under the time-varying control. The dotted lines on Fig. 11 are the quaternion captured by the CCD camera throughout the maneuver. They clearly match the estimated quaternion and confirm the filter convergence.

The second test compares the measured magnetic field values (left-hand side of (9)) with the values calculated using the UKF-estimated quaternion (right-hand side of (9)). They provide a yet another evidence implying the filter convergence under the time-varying control.

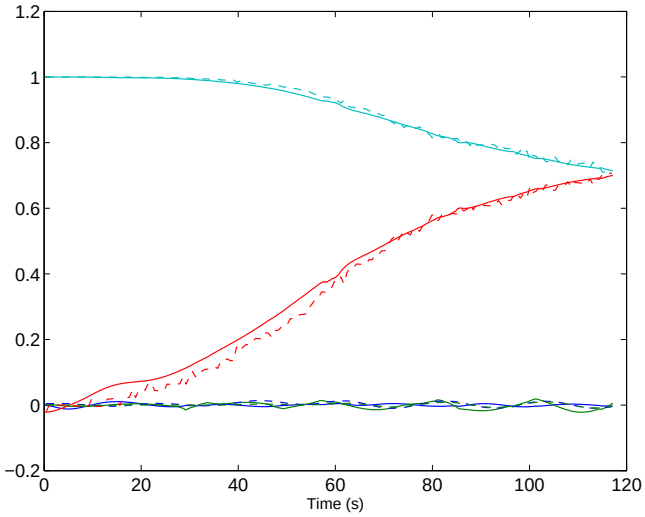

Figure 11. Comparison of the quaternion estimation. Solid lines represent the UKF estimations and dashed lines are the laser diod measurements.

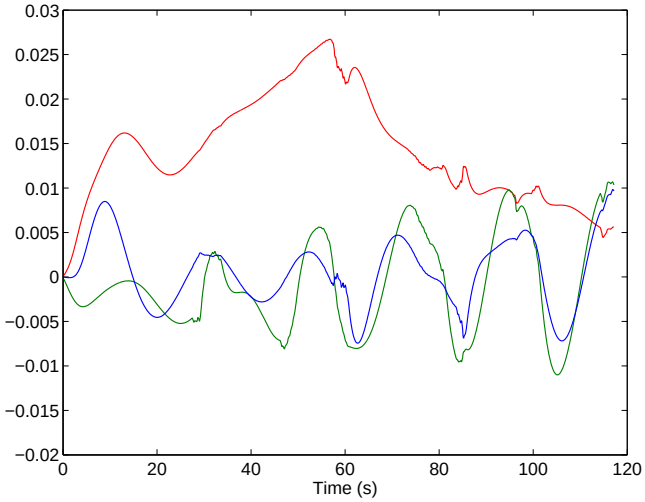

Figure 12. Estimation of the angular velocities by UKF.

VI. Conclusions

NPSAT1 is a gravity-friendly prolate spacecraft that uses active magnetic attitude control. A three-axis magnetometer is the primary onboard sensor that measures the Earth magnetic field during the motion. Magnetometer measurements would then need to be transformed into attitude and angular velocity for control design. In this paper, the Unscented Kalman Filter is designed and experimentally implemented for NPSAT1 attitude estimation. The quaternion unity-norm is enforced through a simple new idea that does not require transformation of four-element quaternion vector into three-element error-quaternion. Instead, the quaternion norm is treated as a dummy output with a "sensed" value of one and augmented into the real sensor measurements. The successful performance of the algorithm is shown through simulations and test experiments. The experiments are conducted on an airbearing test rig that resembles the spacecraft motion in the laboratory environment. Different sets of experiments illustrate the superior performance of the filter under both constant and time-varying control. The convergence of UKF scheme in both cases is validated in various ways including an independent measurement of attitude using an optical measurement system.

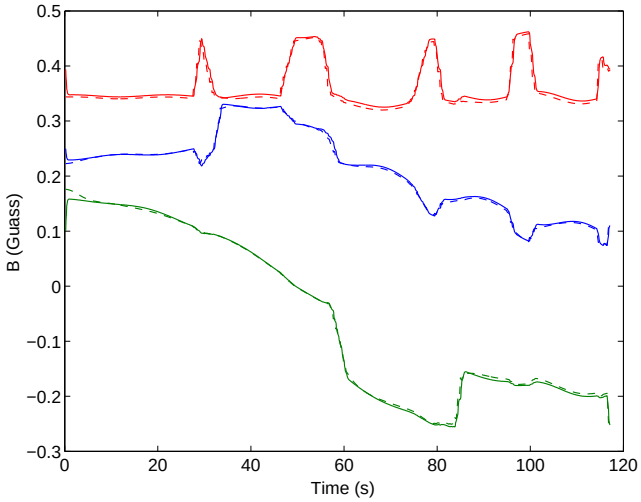

Figure 13. The magnetic field. Solid lines are the measurement from the magnetometer and the dashed lines are the estimated values based on UKF estimated states.

VII. Appendix

A. UKF Algorithm

Consider a general time-varying nonlinear system

$$\begin{aligned} \dot{x} &= f(x,u,t) \\ y &= h(x,t) \end{aligned} \tag{17}$$

where x is the state, u is the control and y is the measurement, respectively. Let sequence $\{t_n\}_{n=0}^{\infty}$ be the sampling time and $x_n = x(t_n)$, $y_n = y(t_n)$.

All Kalman filters have a two-step structure. The first step is to get the prediction of the state, output, denoted as $\tilde{x}_n$, $\tilde{y}_n$, and the covariance matrices:

$$\begin{aligned} \tilde{P}_n^{xx} &= E[(x_n - \tilde{x}_n)(x_n - \tilde{x}_n)^T] \\ \tilde{P}_n^{yy} &= E[(y_n - \tilde{y}_n)(y_n - \tilde{y}_n)^T] \\ \tilde{P}_n^{xy} &= E[(x_n - \tilde{x}_n)(y_n - \tilde{y}_n)^T]. \end{aligned}$$

Once those predictions are calculated, the second step is to correct them using the current measurements. The state is updated according to a simple formula

$$\hat{x}_n = \tilde{x}_n + K(y_n - \tilde{y}_n) \tag{18}$$

where $\hat{x}_n$ is the estimation of $x(t_n)$ and K is called the Kalman gain matrix. By minimizing the trace of the covariance matrix,

$$\hat{P}_n^{xx} = E[(x_n - \hat{x}_n)(x_n - \hat{x}_n)^T],$$

it is easy to show

$$K = \tilde{P}_n^{xy}[\tilde{P}_n^{yy}]^{-1} \tag{19}$$

$$\hat{P}_n^{xx} = \tilde{P}_n^{xx} - K\tilde{P}_n^{xy}K^T. \tag{20}$$

The prediction of the state, $\tilde{x}_n$, is indeed the predication of the mean. Extended Kalman Filter estimates the mean and the covariance by approximating the nonlinear dynamics by a linear one and propagating the mean and covariance to this linear system. Unscented Kalman Filter calculates the prediction of the mean and the covariance with no linearization. The UKF assumes that at every sampling instance, the state x is

always a normally distributed variable. The mean and the covariance information of this random variable can be stored in a set of specially selected points called sigma points. One simple choice of such sigma points is given below[12]

$$\sigma^i \quad = \quad E(x) \pm \sqrt{N_x P},\ i = 1, 2, \ldots, N_x$$

where $E(x)$ is the mean of the random variable x, P is the covariance matrix and N_x is the dimension of x. It can be shown that the nonlinear transformation of the sigma points preserves the system statistics up to the second order in a Taylor series expansion.[12]

Using the above concept, a prediction of the state and the covariance matrices can be carried out as follows

- Based on previous step estimations of the state, $\hat{x}_{n-1}$, and the covariance matrix, $\hat{P}^{xx}_{n-1}$, a set of sigma points can be calculated as

$$\sigma^i \quad = \quad \hat{x}_{n-1} \pm \sqrt{N_x \hat{P}^{xx}_{n-1}},\ i = 1, 2, \ldots, N_x;$$

- Propagate all the sigma points to the nonlinear dynamic with σ_i as the initial condition, i.e.,

$$\begin{aligned} \dot{z} \quad &= \quad f(z, u, t), \\ z(t_{n-1}) \quad &= \quad \sigma_i,\ i = 1, 2, \ldots, N_x; \end{aligned}$$

  and denote $z^i = z(t_n)$, $g^i = h(z^i, t_n)$.

- Calculate the mean (prediction) of the state and the output as

$$\begin{aligned} \tilde{x}_n \quad &= \quad \frac{1}{2N_x} \sum_{i=1}^{2N_x} z^i \\ \tilde{y}_n \quad &= \quad \frac{1}{2N_x} \sum_{i=1}^{2N_x} g^i; \end{aligned}$$

- The prediction of the covariance matrices are calculated by

$$\tilde{P}^{xx}_n \quad = \quad \frac{1}{2N_x} \sum_{i=1}^{2N_x} (z^i - \tilde{x}_n)(z^i - \tilde{x}_n)^T \tag{21}$$

$$\tilde{P}^{yy}_n \quad = \quad \frac{1}{2N_x} \sum_{i=1}^{2N_x} (g^i - \tilde{y}_n)(g^i - \tilde{y}_n)^T \tag{22}$$

$$\tilde{P}^{xy}_n \quad = \quad \frac{1}{2N_x} \sum_{i=1}^{2N_x} (z^i - \tilde{x}_n)(g^i - \tilde{y}_n)^T$$

Once the prediction of $\tilde{x}_n$, $\tilde{P}^{xx}_n$, $\tilde{P}^{yy}_n$ and $\tilde{P}^{xy}_n$ are available, the update is given by equations (18)-(19)-(20).

There are different ways to deal with the process noise and the measurement noise. For instance, one can augment the noises with the state to form a new augmented state vector.[12] This method can take the full advantage of the unscented transformation at the price of increasing computational burden; since more sigma points are generated. In this paper, we assume the process and the measurement noise are purely additive to the model and simply add their covariances to the covariances of the state and the output, i.e., we change the formulas (21)-(22) to the following

$$\begin{aligned} \tilde{P}^{xx}_n \quad &= \quad \frac{1}{2N_x} \sum_{i=1}^{2N_x} (z^i - \tilde{x}_n)(z^i - \tilde{x}_n)^T + Q \\ \tilde{P}^{yy}_n \quad &= \quad \frac{1}{2N_x} \sum_{i=1}^{2N_x} (g^i - \tilde{y}_n)(g^i - \tilde{y}_n)^T + R \end{aligned}$$

where Q and R represent the covariance of the process and measurement noise, respectively.

Acknowledgments

The authors are grateful to Jim Horning, Dan Sakoda and Ron Phelps for their assistance in the experimental setup and interfacing.

References

[1]B. Wie, H. Weiss, and A. Arapostathis, Quaternion Feedback Regulator for Spacecraft Eigenaxis Rotations, *Journal of Guidance, Control, and Dynamics,* Vol. 12, No. 3, 1989, pp. 375-380.

[2]R. Winsniewski and M. Blanke, Fully Magnetic Attitude Control for Spacecraft Subject to Gravity Gradient, *Automatica,* Vol. 35, 1999, pp. 1201-1214.

[3]M. Psiaki, Magnetic Torquer Attitude Control via Asymptotic Periodic Linear Quadratic Regulation, *Journal of Guidance, Control, and Dynamics,* Vol. 24, No. 2, 2001, pp. 386-394.

[4]R. Winsniewski, Linear Time-Varying Approach to Satellite Attitude Control Using Only Electromagnetic Actuation, *Journal of Guidance, Control, and Dynamics,* Vol. 23, No. 4, 2000, pp. 640-647.

[5]P. Wang and Y. B. Shtessel, Satellite attitude control using only magnetorquers, *American Control Conference,* Vol. 1, 1998, pp. 222-226.

[6]B. Leonard, NPSAT1 Magnetic Attitude Control System, *AIAA Smallsat Conference,* 2001, pp. 105-108.

[7]P. Sekhavat, A. Fleming and I. M. Ross, Time-Optimal Nonlinear Feedback Control for the NPSAT1 Spacecraft, *Proceedings of IEEE/ASME International Conference on Advanced Intelligent Mechatronics,* 2005, pp. 843 - 850.

[8]E. J. Lefferts, F. L. Markley and M. D. Shuster, Kalman Filtering for Spacecraft Attitude Estimation, *Journal of Guidance, Control, and Dynamics,* Vol. 5, No. 5, 1982, pp. 417-429.

[9]M. L. Psiaki, F. Martel and P. K. Pal, Three-Axis Attitude Determination via Kalman Filtering of Magnetometer Data, *Journal of Guidance, Control, and Dynamics,* Vol. 13, No 3, 1990, pp. 506-514.

[10]J. K. deutschmann, I. Y. Bar-Itzhack, Evaluation of Attitude and Orbit Estimation Using Actual Earth Magnetic Field Data, *Journal of Guidance, Control, and Dynamics,* Vol. 24, No 3, 2001, pp. 616-623.

[11]M. L. Psiaki and Y. Oshman, Spacecraft Attitude Rate Estimation from Geomagnetic Field Measurements, *Journal of Guidance, Control, and Dynamics,* Vol. 26, No 2, 2003, pp. 244-252.

[12]S. J. Julier and J. K. Uhlmann, Unscented filtering and nonlinear estimation, *Proceedings of the IEEE,* Vol. 92, No. 3, 2004, pp. 401-422.

[13]S. J. Julier, J. K. Uhlmann and H. F. Durrant-Whyte, A new method for the nonlinear transformation of means and covariances in filters and estimator, *IEEE Trans. Automatic. Control.,* Vol. 45, No. 3, pp. 477-482, 2000.

[14]F. Daum, Nonlinear filters: beyond the Kalman Filter, *IEEE A&E Systems Magazine,* Vol. 20, No. 8, 2005, pp. 57-69.

[15]J. L. Crassidis and F. L. Markley, Unscented filtering for spacecraft attitude estimation, *AIAA Journal on Guidance, Control, and Dynamics,* Vol. 26, No. 4, 2003, pp. 536-542.

[16]M. C. VanDyke, J. L. Schwartz, C. D. Hall, Unscented Kalman filtering for spacecraft attitude state and parameter estimation, AAS-04-115, 2004.

[17]E. Kraft, A Quaternion-based Unscented Kalman Filter for Orientation Tracking, *Proceedings of the 6th International Conference on Information Fusion,* Cairns, Australia, 2003, pp. 47-54.

[18]F. L. Markley, Attitude Error Representations for Kalman Filtering, *Journal of Guidance, Control, and Dynamics,* Vol. 26, No 2, 2003, pp. 311-317.

[19]A. Fleming, Real-time optimal slew maneuver design and control, Astronautical Engineer's Thesis, US Naval Postgraduate School, December 2004.

[20]P. C. Wheeler, Magnetic Attitude Control of Rigid, Axially Symmetric Spinning Satellites in Circular Earth Orbits, *NASA Paper CR-313,*, 1971.

[21]D. Holiday, R. Resnick, J. Walker, Fundamentals of Physics, John Whiley and Sons, New York, 2001.